Smart Structures and Systems, *Vol. 16, No. 3 (2015) 415-433*
DOI: http://dx.doi.org/10.12989/sss.2015.16.3.415

A strain-based wire breakage identification algorithm for unbonded PT tendons

A.B.M. Abdullah*, Jennifer A. Rice[a] and H.R. Hamilton[b]

Department of Civil and Coastal Engineering, University of Florida, Gainesville, FL 32611, USA

(Received August 13, 2014, Revised November 20, 2014, Accepted December 2, 2014)

Abstract. Tendon failures in bonded post-tensioned bridges over the last two decades have motivated ongoing investigations on various aspects of unbonded tendons and their monitoring methods. Recent research shows that change of strain distribution in anchor heads can be useful in detecting wire breakage in unbonded construction. Based on this strain variation, this paper develops a damage detection model that enables an automated tendon monitoring system to identify and locate wire breaks. The first part of this paper presents an experimental program conducted to study the strain variation in anchor heads by generating wire breaks using a mechanical device. The program comprised three sets of tests with fully populated 19-strand anchor head and evaluated the levels of strain variation with number of wire breaks in different strands. The sensitivity of strain variation with wire breaks in circumferential and radial directions of anchor head in addition to the axial direction (parallel to the strand) were investigated and the measured axial strains were found to be the most sensitive. The second part of the paper focuses on formulating the wire breakage detection framework. A finite element model of the anchorage assembly was created to demonstrate the algorithm as well as to investigate the asymmetric strain distribution observed in experimental results. In addition, as almost inevitably encountered during tendon stressing, the effects of differential wedge seating on the proposed model have been analyzed. A sensitivity analysis has been performed at the end to assess the robustness of the model with random measurement errors.

Keywords: post-tensioned bridge; unbonded tendon; wire breakage; strain variation; post-tensioning anchorage; multi-strand tendon; damage detection algorithm; automated tendon monitoring

1. Introduction

The use of post-tensioning (PT) tendons is common in long-span segmental box- and I-girder bridge construction, both as external and internal tendons. If not properly protected, these steel tendons corrode over time, resulting in damage; a substantial accumulation of this damage may lead to tendon failure and ultimately bridge collapse. Typically, corrosion protection of tendons is provided by a cement-like filler material, grout, which fills the void in tendon duct. Once hardened, the cementitious grout forms a bond between the tendon and the surrounding concrete. In addition

*Corresponding author, Ph. D. Candidate, E-mail: abm.abdullah@ufl.edu
[a] Assistant Professor, E-mail: jrice@ce.ufl.edu
[b] Professor, E-mail: hrh@ce.ufl.edu

http://www.techno-press.org/?journal=sss&subpage=8 ISSN: 1738-1584 (Print), 1738-1991 (Online)

to providing corrosion protection to the steel, the bonded tendons offer an additional mechanism of tendon force transfer to concrete through the bond, along with the end anchors. However, improper grouting still leads to corrosion (Lau *et al.* 2013) and has caused tendon failures in several post-tensioned bridges (Corven Engineering 2002). These failures have prompted the exploration of an alternative corrosion protection system to the cement grout, such as grease, wax or gel. These flexible fillers do not form bond between tendon and concrete, resulting in an unbonded (or ungrouted) tendon. Although the ultimate strength of unbonded construction is generally less than that of comparable bonded construction, the absence of grout allows easier tendon replacements and improved health monitoring.

As tendon damage can induce serious consequences for structural systems, the development of methodologies to detect the defects or breakage is a subject of much current research. Several monitoring approaches, such as magnetic methods (Scheel and Hillemeier 2003, Wang *et al.* 2000), vibration-based techniques (Tabatabai *et al.* 1998), electrical resistance and electro-mechanical impedance measurement approaches (Nguyen and Kim 2012, Elsener 2008), wave propagation methods (Bartoli *et al.* 2011, Salamone *et al.* 2011, Lanza di Scalea *et al.* 2003, Liu *et al.* 2002, Chen and Wissawapaisal 2001, Matt 2001), have been attempted for defect and breakage detection in prestressing tendons. Among these available methods, acoustic emission (AE) appears to be encouraging and has been successfully implemented in several bridge monitoring applications (Zejli *et al.* 2012, Salamone *et al.* 2012, Fricker and Vogel 2007, Yuyama *et al.* 2007, Cullington *et al.* 2001). However, environmental and traffic noise make the signal identification difficult and the AE system requires sophisticated data processing and filtering to exclude these effects. In addition, appropriate amplifiers and pre-amplifiers are needed to elevate the weak AE signal to a detectable level. Success of other methods in practical applications has been hindered by their short monitoring range, difficulties with operating on a daily basis, insensitivity to tendon defects at initial stage, signal attenuation, accessibility difficulties, high cost, requirements of modifications in the traditional construction detailing and quality control, etc. A more comprehensive listing of the existing monitoring methods with their limitations can be found in Abdullah *et al.* (2014a, b). By utilizing the high strain field over the anchors, the use of unbonded tendons eliminates many of these difficulties with available methods by enabling new monitoring techniques, such as the strain-based approach (Abdullah *et al.* 2014a, b) discussed in this paper.

1.1 Unbonded PT system

Typically, an unbonded PT system has prestressing steel, end anchorages and ducts with a flexible filler material (Fig. 1). The prestressing steel is usually high-strength low-relaxation strand, which consists of seven wires in which six helical wires are wound around a central straight wire (or the king wire). A bundle of strands housed in a plastic sheath forms the tendon.

The PT anchorage consists of an anchor head (or wedge plate), an anchor plate (or bearing plate), and a group of wedges. The anchor head is commonly an iron casting with tapered circular through holes (wedge cavities) to house the wedges and it seats on an anchor plate that bears against the concrete girder. Each wedge is two- or three-part tapered high-strength heat-treated steel that grips the strand in its serrated teeth and holds it in place when seated in an anchor head. The anchorage transmits the tendon force to the concrete and helps maintain the prestress after the stressing jack is removed.

The plastic duct provides a void that permits the installation and stressing of strands. In unbonded construction, the space in the tendon duct is filled with a pliable corrosion protection

system to protect the steel strands from corrosion.

1.2 Strain-based monitoring approach

Because unbonded tendons are connected to the structure only through deviators (components that deviate the path of a tendon to satisfy specific structural needs) and end anchorages, the anchor heads are normally under high prestressing load. A wire break in the strand results in prestress loss and consequently, the strain distribution in the anchor head varies from the unbroken state. This variation of strain field can be used to detect the wire breakage.

The pattern of strain variation depends on the number and location of wire breaks. The anchorage region near the broken strand is more affected by a wire break compared to other region, which results in differential strain variation among the monitoring points (strain gauge locations) around the anchor head perimeter. This inequality increases with the distance of the broken strand from the anchor center, i.e., a wire break in an outer layer strand (Fig. 2) produces a higher relative strain variation than a breakage in an inner layer. Again, because of proximity to the monitoring points, a larger strain drop occurs for breakages on the outer layer strands in contrast to the inner layers. Moreover, the quantity of strain drop increases with the number of wire breaks, indicating the severity of damage. A proof-of-concept study on this monitoring approach can be found in earlier work (Abdullah *et al.* 2014a), which introduces the strain-based method and primarily investigates its feasibility through a calibrated finite element model.

This paper provides experimental validation of the previously proposed method by evaluating the levels of strain variation measured in different directions on the anchor head with various damage scenarios. After validating the responsiveness of strain distribution in anchor head to tendon damage, a promising wire breakage detection algorithm has been presented to characterize the damage programmatically. Finally, an error sensitivity study is carried out to verify the robustness of the proposed model.

2. Experimental program

An experimental program was undertaken to study the changes in strain distribution in the anchor head due to wire breaks. Although it is likely that the outer strands will be more susceptible to corrosion and fretting fatigue in in-field conditions, wire breaks may potentially occur in any strand layer. The program, therefore, included three sets of tests, where each set involved stressing and cutting each of the wires of the center and a non-center strand on different layers. The resulting strain in a 19-strand anchor head was continuously measured with a group of strain gauges installed at different locations on the external surface of the anchor head (Fig. 2). The state of strain at pristine condition was then compared with the strains after different numbers of wire breaks to calculate the corresponding strain variation.

2.1 Test setup

An approximately 1.5 m (5 ft) long steel reaction fixture (Fig. 2) was used to react against the applied load in the strands. A stiffened anchor plate was placed at the stressing end of the fixture to bear an anchor head, whereas a load cell was positioned between the end bearing plate and the anchor plate at dead end. The strands were passed through a longitudinal conduit located at the

center of the fixture and was anchored to the dead end anchorage. The other end of the strands was held by the grippers of a hydraulic jack for tensioning and was finally anchored to the stressing end anchorage. An opening near the stressing end allowed access to the strands for cutting.

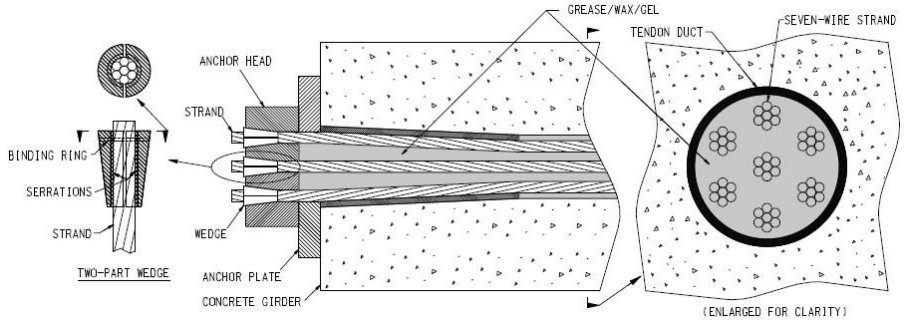

Fig. 1 Multi-strand unbonded PT system

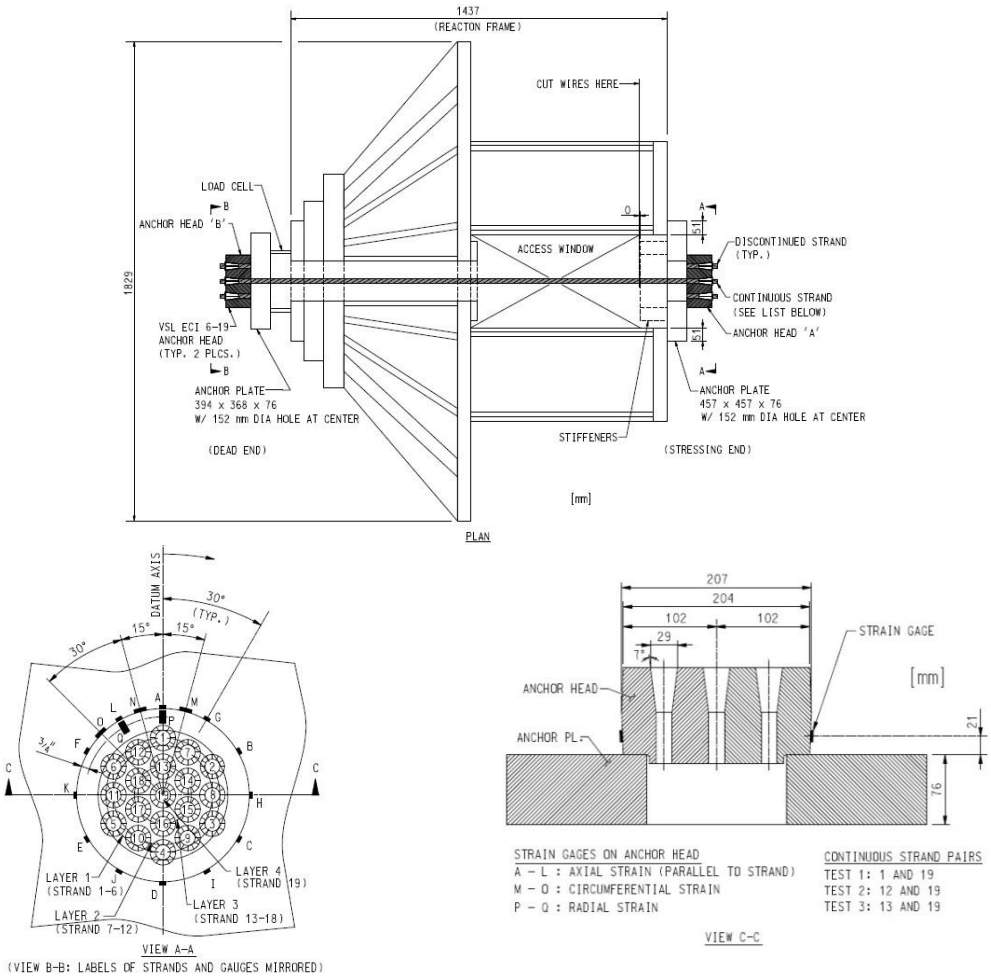

Fig. 2 Reaction fixture details and sensor layout

15.2 mm (0.6 in) diameter Grade 270 strands, conforming to ASTM A416 (ASTM 2006), were used in this experiment. The low-relaxation seven-wire strands were approximately 2.75 m (9 ft) long with a cross sectional area of 140 mm^2 (0.217 in^2). The PT anchorage comprised a 19-strand anchor head (VSL ECI 6-19, VSL International, Köniz, Switzerland) sitting on a 76 mm (3 in) thick anchor plate at each end. The wedge cavities in the anchor heads accommodated two-part wedges.

Seventeen foil strain gauges (gauge length of 5 mm) were installed on each of the two anchor heads (Fig. 2); twelve (A-L) to measure axial strain, three (M-O) for circumferential strain and two (P-Q) for radial strain. A donut load cell was placed at the dead end of the reaction fixture to monitor the total tendon force during the entire duration of stressing and cutting phase. In addition, six foil strain gauges (gauge length of 0.5 mm) were installed on wires to estimate the individual strand load during stressing.

The equipment used for stressing the tendon consisted of a mono-strand jack, a calibrated pressure gauge and a hydraulic pump. To manually introduce wire breaks, the wires were mechanically cut with a Dremel® high-speed rotary tool. Relatively small diameter (31.75 mm), fiberglass-reinforced cutoff wheels were used to facilitate separate wire cuts. A Dremel® flexible shaft attached to a specially designed guiding rod with an adjustable clamp helped in cutting the stressed wires through the access window from a safe distance (Fig. 3).

2.2 Experiment

In each of the three sets of test, two strands were stressed during the experiment (Fig. 4). Table 1 lists the amount of tension applied to each of these strands. A larger load could not be achieved due to high seating loss in short tendons. Because of limitations of the reaction fixture, the remaining strands were not continued to the other end but the wedges on both of the anchor heads were preseated by stressing the respective strands to approximately 74% of their ultimate strength (0.74 F_u). Although the anchor plates were under less-than-practical stress levels (as all the strands were not continued to the other end), the fully populated anchor heads with preseated wedge provided a reasonable test condition to examine the state of strain.

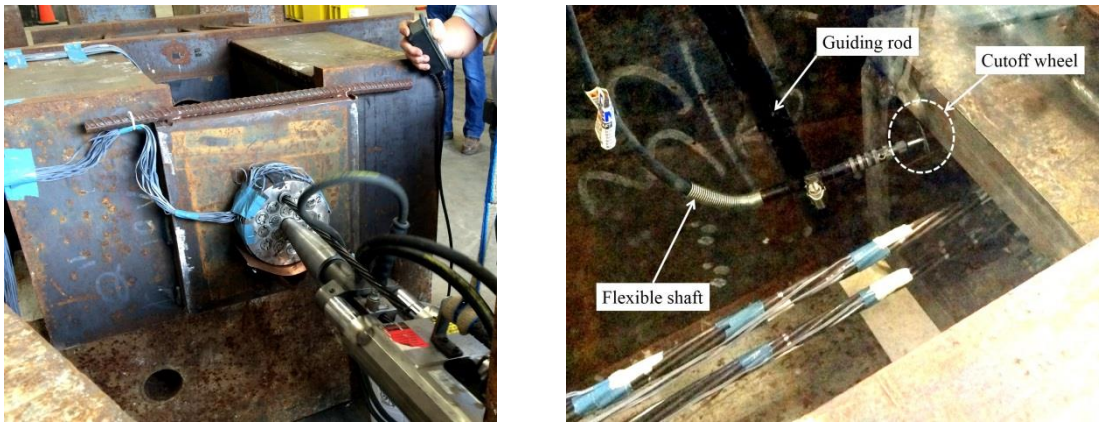

(a) Stressing (b) Cutting

Fig. 3 Tendon stressing and cutting apparatus

Table 1 Test matrix and loading scheme

Test ID	Strand/Wedge label (Fig. 2)	Applied load	
		kN (kip)	% of F_u
1	Strand 1	101.0 (22.7)	39%
	Strand 19	131.7 (29.6)	51%
	Preseated wedge 2-18	193.0 (43.3)	74%
2	Strand 12	114.8 (25.8)	44%
	Strand 19	135.7 (30.5)	52%
	Preseated wedge 1-11, 13-18	193.0 (43.3)	74%
3	Strand 13	110.8 (24.9)	42%
	Strand 19	130.3 (29.3)	50%
	Preseated wedge 1-12, 14-18	193.0 (43.3)	74%

(a) Test frame

(b) Stressing end

Fig. 4 Experimental setup

In *Test 1*, tension was gradually applied to the center strand (strand 19) with a mono-strand jack, followed by the non-center strand (strand 1). The effective loads in individual strands were measured by a pressure gauge attached to the jack and foil strain gauges installed on wires, along with the total tendon force reading from the load cell. After achieving the target stress level in each of the strands (Table 1), the wires of strand 1 were gradually cut until the complete breakage of the strand was achieved. After cutting all the wires in strand 1, the wires in strand 19 were cut. The resulting strains in both anchor heads were recorded during the entire duration of stressing and cutting phase with sampling frequency of 10 Hz and 100 Hz, respectively. Stressing and cutting of other strands in *Test 2* and *Test 3* were carried out by following a similar procedure. Fig. 5 shows representative time histories of measured strains during cutting.

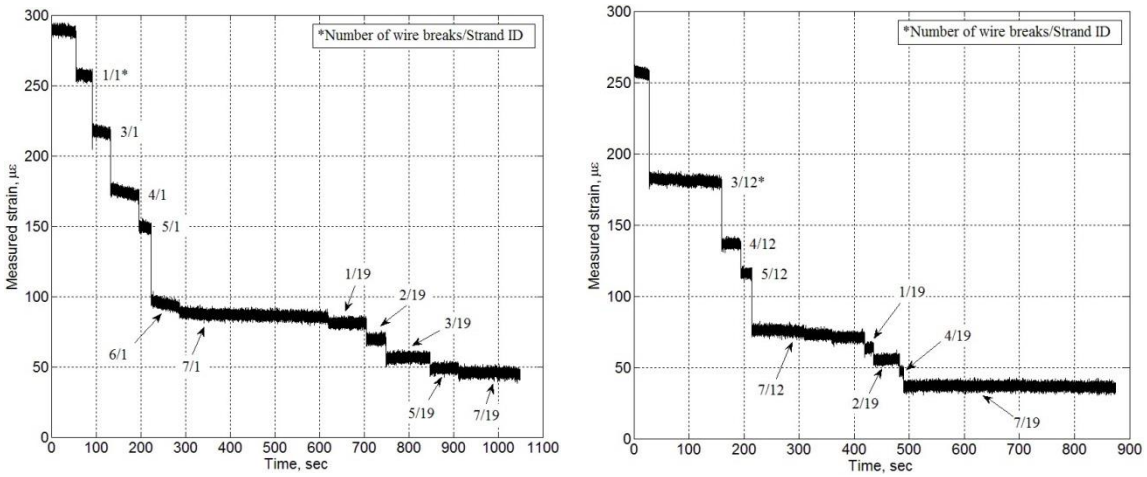

(a) Test 1: wire breaks in strand 1 and 19 (b) Test 2: wire breaks in strand 12 and 19

Fig. 5 Time history of measured strains by gauge L

2.3 Results

Under the loading and boundary conditions, the resulting strain in an anchor head is expected to develop primarily in three directions: axial (because of tension in strands), circumferential and radial (because of wedge seating in anchor head). The strain response in all these three directions was captured to assess the sensitivity of measured strains to wire breaks.

2.3.1 Axial strains

Because of wire breaks in strand 1 on the outermost layer, the maximum axial strain drop was experienced by strain gauge A (closest gauge to the broken strand), followed by the adjacent gauges, and the magnitude of strain drop increased with the number of wire breaks (Fig. 6). Similarly, in case of *Test 2*, where wire breaks occurred in strand 12 on layer 2, gauge L (closest gauge to strand 12) captured the highest strain drop and as expected, strain relief increased with each subsequent wire break. Observations in *Test 1* and *Test 2* held in *Test 3*, where wire breaks occurred in strand 13 on layer 3. Gauge A, which was the closest gauge to broken strand 13, recorded the greatest strain drop and the extent of strain drop increased monotonically with the number of wire breaks. Additionally, larger strain drops occurred for wire breaks in outer layer strands compared to the inner layer, noting that all the three non-center strands (strand 1, 12 and 13) were almost equally stressed (ranging from 0.39 to 0.44 F_u). However, Figs. 6(a)-6(c) show unequal strain variation at two symmetric locations about the broken strand, which is likely due to unequal seating of wedge parts (designated as differential wedge seating in this paper) as is discussed later. In case of wire breaks in the center strand 19, the strain decreased at all monitoring points by a small amount; however, as all the gauges were equidistant from the broken strand, no distinct peak/trough was observed in the strain variation plot.

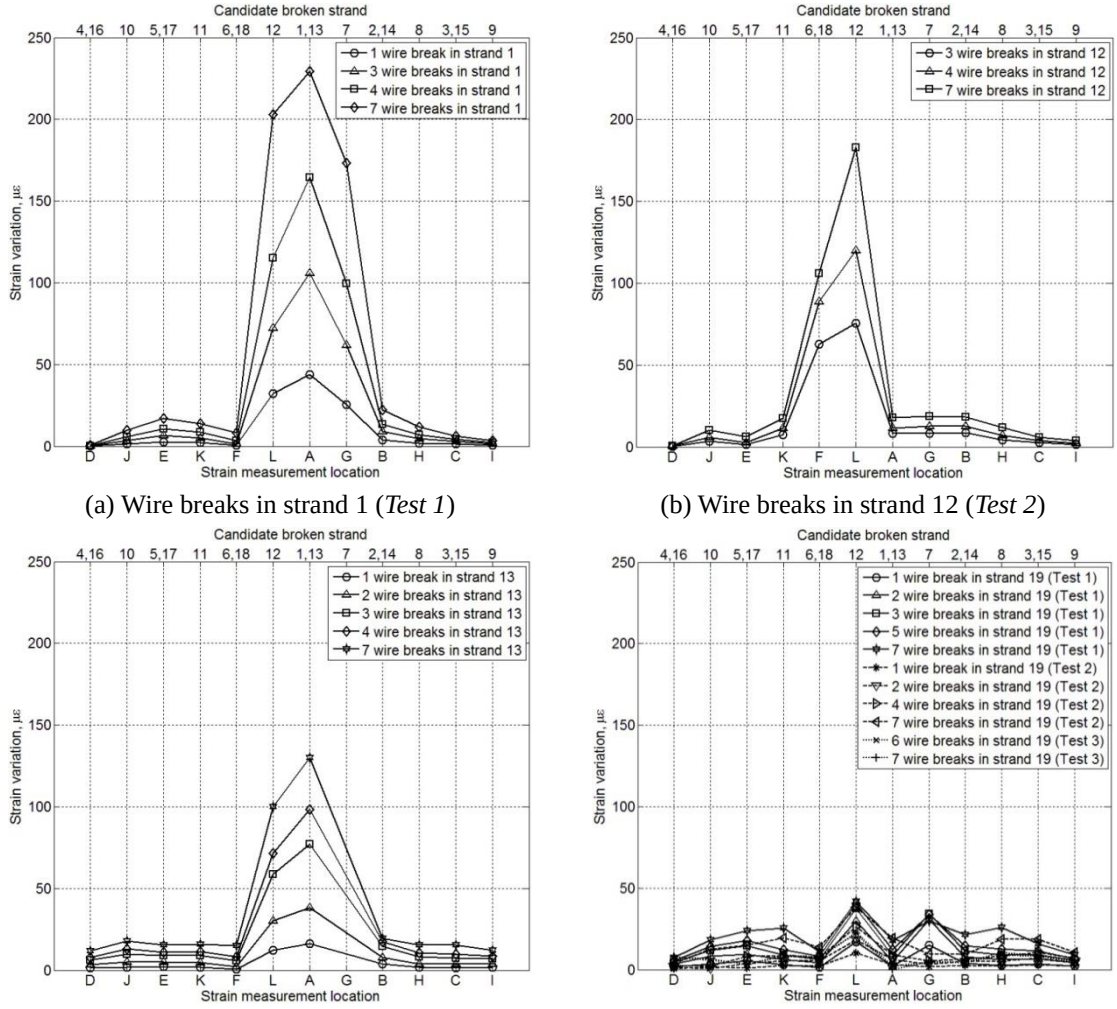

(a) Wire breaks in strand 1 (*Test 1*) (b) Wire breaks in strand 12 (*Test 2*)

(c) Wire breaks in strand 13 (*Test 3*) (d) Wire breaks in the core strand (strand 19)

Fig. 6 Axial strain variations due to wire breaks

2.3.2 Circumferential and radial strains

Circumferential strains, measured by gauge M, N and O (Fig. 2), decreased consistently with wire breaks in both non-center (strand 1, 12 and 13) and center (strand 19) strands (Fig. 7); however, the magnitude of the strain decreases were less than that of axial strains. Furthermore, radial strains, captured by gauge P and Q, were the least sensitive among the three groups of strain measurement (Fig. 8). Although relatively small, the strain variations were consistent with the number of wire breaks. Thus, both circumferential and radial strains were found less sensitive compared to axial strains. This is due to the fact that the tendon force transfers from anchor head to anchor plate mainly through bearing, which results in high axial compressive strain in anchor head. The tensile circumferential strains and compressive radial strains occur only due to the widening of anchor head resulting from seating of wedges into the conical hole through frictional contact.

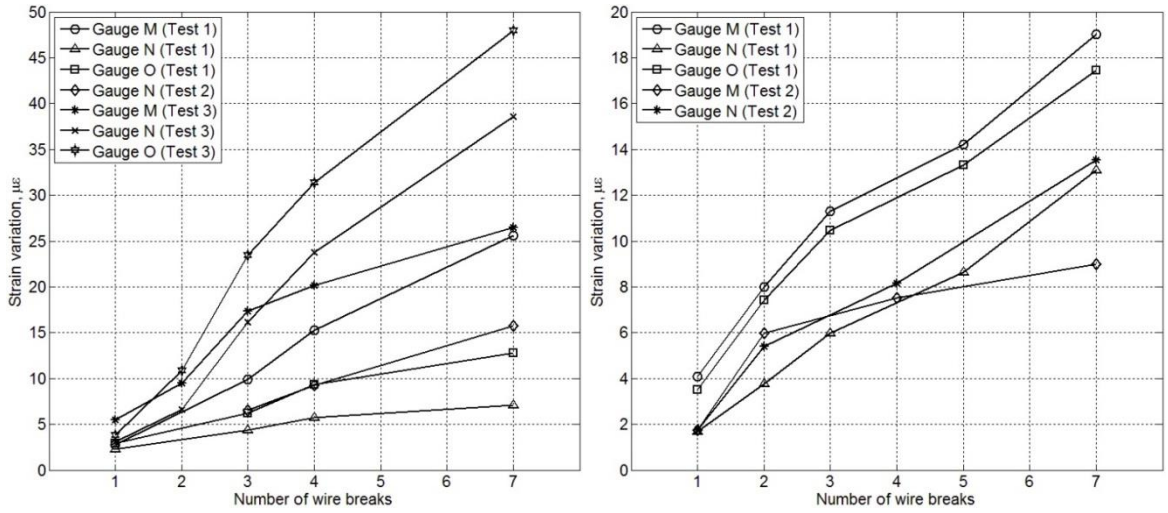

(a) Wire breaks in non-center strands (b) Wire breaks in center strands

Fig. 7 Circumferential strain variations due to wire breaks

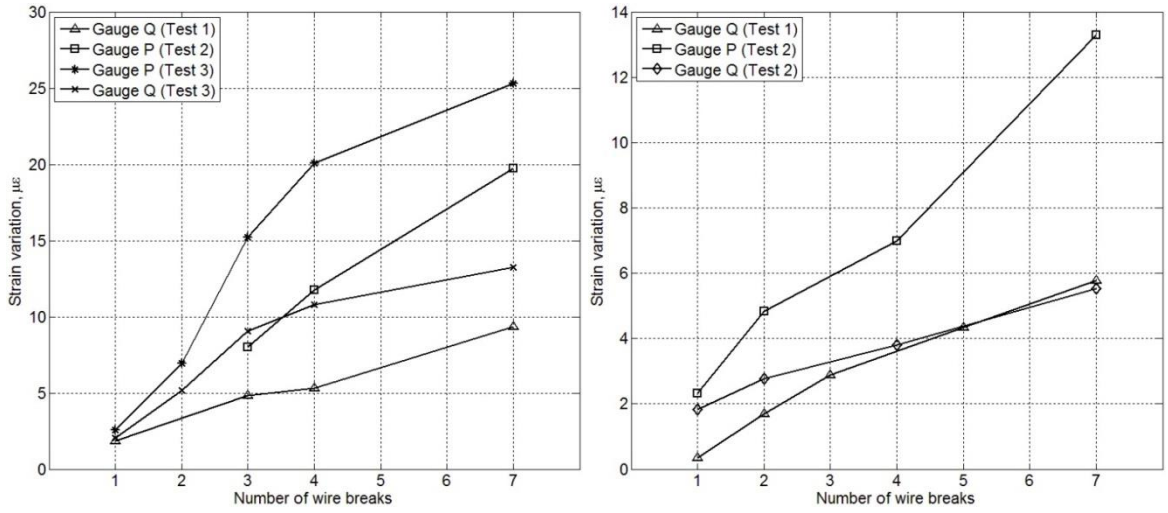

(a) Wire breaks in non-center strands (b) Wire breaks in center strands

Fig. 8 Radial strain variations due to wire breaks

It is noted that identical strain variations were observed at most of the matching gauges in the two anchor heads, except some anticipated discrepancies due to dissimilar support conditions of the two anchor plates. In this paper, the measured strains in anchor head 'A' have been reported. However, although preliminary protective measures were taken, a few gauges debonded and/or disconnected during the testing; results from those non-functioning gauges are not reported. This

gauge debonding issue highlights the importance of a rigorous investigation on durability of gauges for long-term monitoring, such as exploring a more effective gauge protector or examining the practicality of embedding the gauges into the anchor head.

The experimental program conducted on a partially-stressed anchor head, thus confirms the detectability of wire breaks from the measured strain variations in the anchor head and identifies axial strain as the most sensitive damage indicator. However, a parametric study with other breakage conditions under more practical tendon loads is necessary to illustrate the damage detection algorithm. The next section, therefore, discusses the development of finite element (FE) model of an anchorage for additional algorithm assessment.

3. FE model of PT anchorage

An FE model of a 19-strand anchorage (VSL E 6-19) was prepared to calculate the strain variations for various wire breakage scenarios. As an attempt to simulate realistic conditions, an effective prestress load of 0.63 F_u (0.80 F_u minus an estimated short- and long-term losses) was considered at undamaged state. The FE results have been used in the subsequent sections to construct a wire breakage detection algorithm as well as to investigate the observed asymmetry in experimentally measured strain distribution.

The model, however, must consider the complex mechanical behavior of the anchorage under heavy prestressing loads, because the loading mechanism of wedge seating into the anchor head give rise to a frictional contact problem. In addition, the model must take into account plasticity, large displacement and other contact non-linearities. To account for the contact problem originating from the interactions of wedge-anchor head and anchor head-anchor plate interfaces, the FE model was calibrated with friction coefficients at the two interfaces. A detailed description of the calibration procedure can be found in earlier works (Abdullah *et al.* 2014a), where the friction coefficients at the wedge-anchor head and the anchor head-anchor plate interfaces were as 0.015 and 0.1, respectively. Augmented Lagrangian and Penalty formulations were used in normal and tangential directions, respectively, to enforce compatibility at the contact interfaces. Different components of the anchorage (anchor head, anchor plate and wedges) were discretized with 20-node quadratic hexahedral and 10-node quadratic tetrahedral continuum elements. A simplified model of the wedge was considered assuming that the two parts act monolithically and was replaced by a single equivalent wedge component. In addition, the strand was not explicitly modelled but the wedge was laterally constrained and the wedge cavity was assumed to be very stiff to ensure unidirectional wedge seating. A displacement-controlled loading scheme was employed through wedge seating and an idealized pinned boundary condition was considered to support the bearing plate. More details on selecting appropriate FE parameters for the anchorage model can be found in literature (Marceau *et al.* 2011, Bastien *et al.* 2007, 1996).

Because axial strain was found to be the most sensitive strain to wire breakage, the FE model (and the subsequently developed damage detection algorithm) only considers axial strains to study the pattern of strain variations among the 12 monitoring points shown in Fig. 9(a). The numerical calculations confirmed strain variation in anchor head under a realistic loading condition. Larger strain variation occurred due to wire breaks in outer strands than inners and the magnitude of variation decreased at monitoring points away from the broken strand. Representative FE results for wire breakages in different strand layers are depicted in Fig. 9(b).

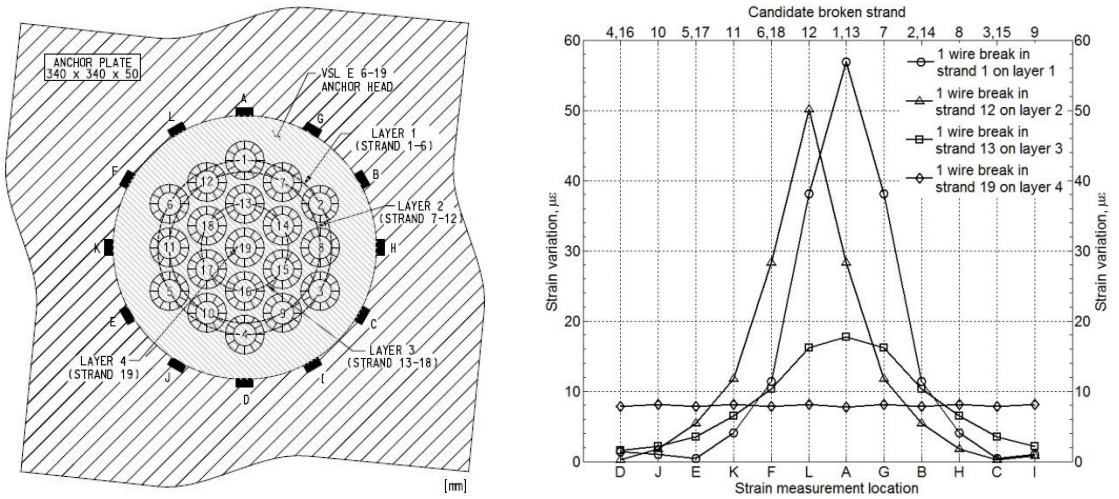

(a) Strand and monitoring locations (b) Strain variations for wire breaks at different layers

Fig. 9 Monitoring locations and representative strain variations from FE analyses

4. Wire break detection algorithm

This section introduces a damage detection model suitable for an automated tendon monitoring application. The model is capable of detecting single or multiple wire breaks in the same strand; however, the more challenging single wire break condition has been considered for demonstration. FEA results of a fully-stressed E 6-19 anchor head, obtained in the previous section, have been used to illustrate the algorithm. The robustness of the model has been preliminarily tested through a sensitivity study with random measurement errors.

4.1 Underlying framework

A wire break in an outer layer strand produces a sharper peak in strain variation plots compared to the inner layers; e.g., breakages in strand 1 and 12 result in a narrow peak, whereas breakage in strand 13 yields a wider plot (extended over a larger region) with smaller peak, and that in core strand produces a mostly flat plot (Fig. 9). These characteristics of strain plots represent a dissimilar strain variation among the monitoring points, which are used to calculate two damage-sensitive parameters: the peak percentage strain variation (p) and the peak relative percentage strain variation (r). These parameters are then checked against a group of preset thresholds (ϕ, γ, λ, ψ) to verify a breakage event and to select a pool of candidate strands by identifying the strand layer on which the broken wire lies. After selecting the candidate strands, strain variations at all the monitoring points are considered to identify the broken strand. As each strand is located at different distance from the strain monitoring points, the calculated strain variations are normalized by the distances between the monitoring points and the strand. The maximum of these normalized strain variations, designated as the damage index (DI) in this paper, is calculated for each of the candidate strands and the maximum damage index (DI_{max}) determines the broken strand.

4.2 Damage parameters and thresholds

The proposed model incorporates several key parameters and thresholds in developing the wire breakage detection algorithm. A list of these parameters and thresholds is provided as follows:

$(\varepsilon_i)_b$: Calculated strain at monitoring point i before the occurrence of wire breakage

$(\varepsilon_i)_a$: Calculated strain at monitoring point i after the occurrence of wire breakage

$\Delta\varepsilon_i$: Percentage strain variation at monitoring point i

p : Peak percentage strain variation

r : Peak relative percentage strain variation

ϕ : Threshold to assess the occurence of wire break

γ : Upper bound of parameter r to identify the breakage occurred in layer 1

ψ : Lower bound of parameter p to identify the breakage occurred in layer 2

λ : Upper bound of parameter r to identify the breakage occurred in layer 3

DI_j : Damage index for strand j

d_{ij} : True distance between monitoring point i and strand j

$DI_{\max}$: Maximum damage index

The above parameters have been calculated in different steps of the algorithm using the following equations

$$\Delta\varepsilon_i = \frac{(\varepsilon_i)_a - (\varepsilon_i)_b}{(\varepsilon_i)_b} \times 100 \tag{1}$$

$$p = \max(\Delta\varepsilon_i) \tag{2}$$

$$r = \max\left(\frac{\Delta\varepsilon_i}{\max(\Delta\varepsilon_i)}\right) \tag{3}$$

$$DI_j = \max\left(\frac{\Delta\varepsilon_i}{d_{ij}}\right) \tag{4}$$

$$DI_{\max} = \max(DI_j) \tag{5}$$

4.3 Algorithm development

The various stages where different parameters and thresholds were introduced into the model are summarized in Fig. 10 followed by a stepwise description of the algorithm.

Step 1: Wire break occurrence assessment

a) Peak percentage strain variation calculation

First, the peak percentage strain variation (p) among the six monitoring points 'A' to 'F' is calculated using Eqs. (1) and (2). Because of the relative positions of the strands and monitoring points, it has been found that considering the strain variations at these six non-adjacent points, in place of 12, is more effective in establishing widely spaced thresholds to differentiate closely located strand layers, such as layer 1 and 2. After identifying the candidate strands, however, all the 12 monitoring points have been taken into account to calculate the damage indices.

b) Threshold check

The occurrence of a wire breakage event is then confirmed by checking the parameter p against the threshold ϕ as shown in Fig. 10.

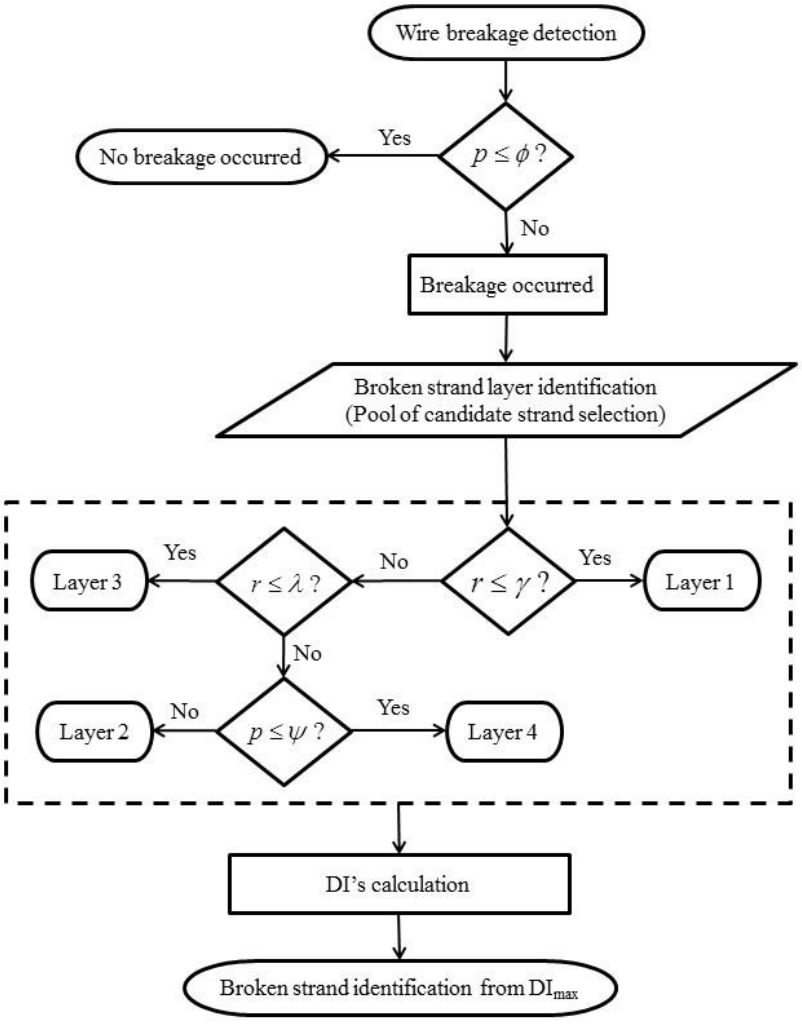

Fig. 10 Wire breakage identification flowchart

Step 2: Broken strand layer identification

a) Peak relative percentage strain variation calculation

If *Step 1* indicates that a breakage has occurred, then the peak relative percentage strain variation (r) is calculated among the six monitoring points 'A' to 'F' using Eqs. (1) and (3).

b) Threshold check

The parameter r is then compared to thresholds γ and λ to identify the broken strand layer. An additional threshold ψ has been found necessary for layers 2 and 4 to check against parameter p calculated in *Step 1* (Fig. 10).

Step 3: Broken strand detection

a) Damage index calculations

After identifying the broken strand layer in *Step 2*, a damage index, *DI*, is calculated for each of the strands on that layer from Eq. (1) and (4) considering all the 12 monitoring points ('A' to 'L').

b) Locating the breakage

Finally, the strand associated with the maximum of all the calculated damage indices (DI_{max}) is identified as the broken strand.

It is noted that, although the *DI's* indicate the relative likelihood of wire breakage in individual strands on the identified layer, there is no explicitly defined threshold for *DI* that a strand must exceed to be determined as broken. This is because the *DI's* are calculated only if a breakage is confirmed by satisfying the criterion that the peak percentage strain variation (p) exceeds the threshold ϕ in *Step 1*. Moreover, additional thresholds (γ, λ, ψ) are incorporated in *Step 2* to identify the broken strand layer. Thus the *DI's* inherently entail several thresholds and the model, therefore, identifies the broken strand by picking the maximum damage index (DI_{max}) and disregards the rest of the *DI's*. However, the individual and/or relative magnitudes of the damage indices (*DI's*) may indicate wire breaks occurring in different strands.

4.4 Error sensitivity analysis of the damage detection model

A preliminary test with a pre-determined set of thresholds has been performed to evaluate the robustness of the model in the presence of random measurement errors. Some artificial errors were assigned to the original strain measurements and the detectability of wire breaks was then estimated through Monte Carlo simulation.

4.4.1 Determination of thresholds

A parametric study was conducted on E 6-19 anchor head to investigate the strain distribution for all possible single wire breakage conditions. From this study, the thresholds defined previously were selected as follows:

$\gamma = 0.4$; $\lambda = 0.7$; $\psi = 1.0$; $\phi = 0.5$

It is noted that these thresholds have been used only to assess the performance of the model

with limited measurement errors and cannot be utilized universally. Individual thresholds will vary with the type of anchor head and need to be adjusted to cope with in-field noise and measurement errors. This will require a long-term statistical data of in-field noise associated with the strain measurements and a realistic estimation of all the measurement uncertainties due to environmental and traffic loads, differential wedge seating and other non-breakage events, to refine the thresholds and achieve a target detectability under the given field conditions.

4.4.2 Sensitivity study of measurement errors

Systematic errors may occur in strain measurements due to fabrication faults in strain gauges along with random errors due to gauge misalignment, transverse sensitivity of gauges, or differential temperature at monitoring locations. In addition, differential wedge seating may cause somewhat irregular strain distribution (discussed in the following section). The sensitivity of the proposed model to these imperfections and unevenness has been tested with uniformly distributed pseudorandom errors.

Table 2 Success rate of single wire break identification

Broken strand ID	Strand layer	Simulation I		Simulation II		Simulation III	
		Error range, $\mu\varepsilon$	Success rate of detection (95% CI*)	Error range, $\mu\varepsilon$	Success rate of detection (95% CI)	Error range, $\mu\varepsilon$	Success rate of detection (95% CI)
1	Layer 1	-6.0 to +6.0 (in all gauges)	98-99	-9.5 to +9.5 (in all gauges)	80-85	-10.0 to +10.0 (in two random gauges) and -2.0 to +2.0 (in the rest of the gauges)	96-98
2			98-99		81-85		97-99
3			98-99		82-87		97-99
4			97-99		81-85		97-99
5			98-99		81-86		96-98
6			98-99		81-86		97-99
7	Layer 2		84-88	-6.0 to +6.0 (in all gauges)	84-88		91-95
8			80-85		80-85		91-94
9			81-86		81-86		90-94
10			80-85		80-85		90-93
11			80-85		80-85		91-94
12			83-88		83-88		91-95
13	Layer 3		26-32	-1.5 to +1.5 (in all gauges)	80-85		46-52
14			36-42		84-88		54-60
15			25-30		83-88		47-50
16			33-39		81-86		50-56
17			31-37		84-88		49-56
18			32-39		83-87		57-63
19	Layer 4		12-16	-2.0 to +2.0 (in all gauges)	85-89		58-64

*CI: Confidence interval

Three sets of Monte Carlo simulations were conducted with a sample size of 1000; in *Simulation I*, errors ranging from -6.0 to +6.0 $\mu\varepsilon$ were randomly added to all the strain measurements. Tolerance limits for different strand layers were determined in *Simulation II* to achieve a target detectability of at least 80%. In *Simulation III*, higher errors (-10.0 to +10.0 $\mu\varepsilon$) were added to two randomly selected gauges than the remainder of gauges (error range: -2.0 to 2.0 $\mu\varepsilon$). As expected, the simulation results show less false negatives, hence higher detectability of wire breaks, in outer layer strands compared to the inner layers (Table 2). However, it is noted that the error levels were selected to test the model under certain measurement uncertainties; a more refined error sensitivity analysis with in-field measurements has been planned and the current model is to be applied to the experimental data with more realistic measurement errors.

5. Effects of differential wedge seating on the proposed model

From the experiments, axial strain variations were clearly observed with wire breaks in case of non-center strands. For example, in *Test 1* (Fig. 6(a)), the closest gauge to the broken strand 1 (gauge 'A') captured higher strain variations relative to other gauges. The plot, however, is not symmetric about point A; e.g., strain variations measured by two symmetrically placed gauges L and G are not equal. A finite element analysis implies that this asymmetry may be attributed to differential wedge seating (unequal seating of the two wedge parts) along with other factors, such as gauge misalignments. To investigate this, the FE model described in earlier sections in this paper with a single equivalent wedge component was modified. In this revised model, the two wedge parts were allowed to slide over one another assuming frictionless interactions at their interfaces. Fig. 11(b) shows a comparison of strain variations between an ideal equal wedge seating and a differential wedge seating condition. In both cases, a single wire break was considered in strand 4 and the unequal wedge seating was conducted with 5% differential seating between the two wedge parts.

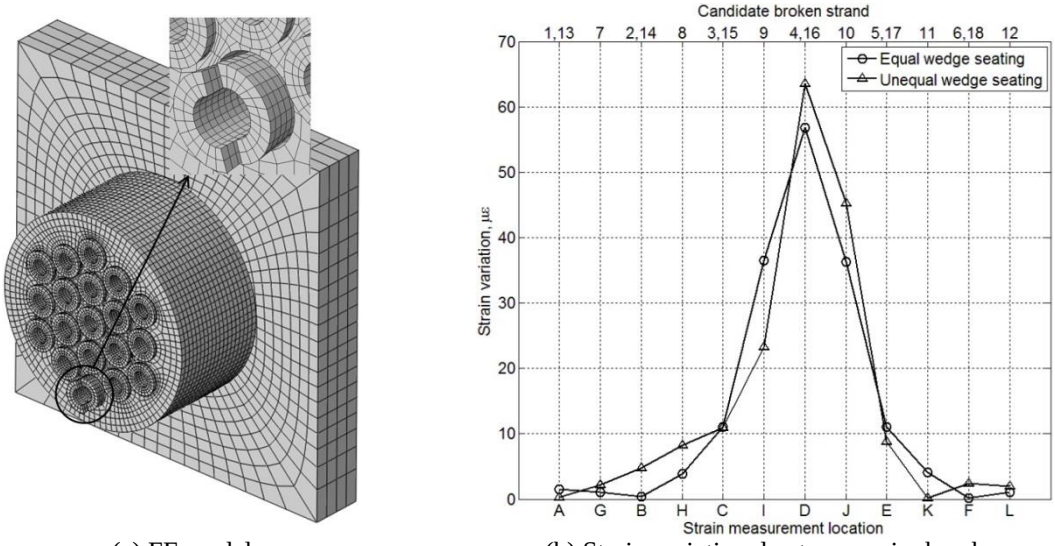

(a) FE model (b) Strain variation due to one wire break

Fig. 11 Differential wedge seating

Although the differential wedge seating for a single strand appears to create some uneven strain distribution, many of these individual effects are likely to mitigate each other when considering all the wedges in a fully populated anchor head. This combined effect of differential wedge seating has been regarded as one of the random measurement uncertainties in the previous section. A more practical assessment of this effect along with other measurement errors will be pursued in future experiments.

6. Conclusions

A wire breakage experiment has been conducted to study the sensitivity of strain response in anchor head under various damage conditions. Strain distributions along external surfaces of the anchor head (in axial, circumferential and radial directions) have been reported for various wire breakage scenarios. Following this experiment, a promising damage detection model has been introduced. Strain variations for a broad spectrum of wire breakage conditions were obtained from FEA and the results were used in estimating the thresholds in the damage detection model. The susceptibility of the model to in-field conditions have been preliminarily tested with artificially generated random measurement errors. Different combinations of measurement uncertainties were incorporated into the model and detectability of wire breaks were estimated from simulation results.

The experimental results confirmed the presence of strain variations due to wire breaks as well as the occurrence of the maximum axial strain drop at the closest monitoring location. As expected, the extent of strain drop consistently increased with the number of wire breaks and a larger strain decrease occurred due to breakage in an outer strand. In addition, axial strain has been found to be the most sensitive strain to wire breaks and radial strain to be the least. The proposed model performed well with randomly selected measurement errors, showing higher detectability of breakage in outer strands. The method allows a simple data processing algorithm to obtain a robust damage detection model suitable for automated long-term implementation and overcomes many of the challenges faced by the available approaches through the use of low-cost, easy to install sensors and an off-the-shelf data acquisition system.

Relatively low detectability, however, was observed in cases of single wire breakage in inner layer strands because they resulted in small strain variations. Locating such breakages in in-field conditions with the presence of ambient noise is expected to be difficult; however, multiple wire breaks in the strand would increase the detectability. An estimation of in-field measurement noise along with the effects of differential temperature and wedge seating on a fully-loaded anchor head is necessary to assess the detection uncertainties and to adjust the thresholds associated with the current model. In addition, field deployment of this monitoring approach is required to consider time-dependent prestress loss originating from strand relaxation, durability of gauges for long-term installation and the influence of deviation points and recovery lengths on strain measurement.

Acknowledgements

The research project is supported by the Florida Department of Transportation (FDOT) under Contract No. BDV31-977-15. The authors express special thanks and appreciation to William Potter and the support team at FDOT's M. H. Ansley Structures Research Center for their

collaboration in conducting the experiment reported in this paper. The opinions and findings are those of the authors and not necessarily those of the sponsors.

References

Abdullah, A.B.M., Rice, J.A. and Hamilton, H.R. (2014a), "Wire breakage detection using relative strain variation in unbonded posttensioning anchors", *J. Bridge Eng.*, 10.1061/(ASCE)BE.1943-5592.0000639, 04014056.

Abdullah, A.B.M., Rice, J.A. and Hamilton, H.R. (2014b), "A damage detection model for unbonded post-tensioning tendons based on relative strain variation in multi-strand anchors", *Proceedings of the SPIE Sensors and Smart Structures Technologies for Civil, Mechanical, and Aerospace Systems*, San Diego, CA, March.

ASTM. (2006), "Standard specification for steel strand, uncoated sevenwire for prestressed concrete", *A416*, West Conshohocken, PA.

Bartoli, I., Salamone, S., Phillips, R., Lanza di Scalea, F. and Sikorsky, C.S. (2011), "Use of interwire ultrasonic leakage to quantify loss of prestress in multiwire tendons", *J. Eng. Mech. - ASCE*, **137**(5), 324–333.

Bastien, J., Marceau, D., Fafard, M. and Chabert, A. (1996), "Experimental and numerical study of multi-strands wedge anchor heads", *Symposium on Post-Tensioned Concrete Structures*, Concrete Society, Slough, U.K.

Bastien, J., Marceau, D., Fafard, M. and Ganz, H.R. (2007), "Use of FEA for design of posttensioning anchor head", *J. Bridge Eng.*, **12**(2), 194-204.

Chen, H.L.R. and Wissawapaisal, K. (2001), "Measurement of tensile forces in a seven-wire prestressing strand using stress waves", *J. Eng. Mech. - ASCE*, **127**(6), 599-606.

Corven Engineering (2002), *New directions for Florida post-tensioned bridges: Vol. 1: Post-tensioning in Florida bridges*, Technical Report, Florida Department of Transportation (FDOT), Tallahassee, FL, Available at http://www.dot.state.fl.us/structures/posttensioning.shtm

Cullington, D.W., MacNeil, D., Paulson, P. and Elliott, J. (2001), "Continuous acoustic monitoring of grouted post-tensioned concrete bridges", *NDT&E Int.*, **34**(5), 95-105.

Elsener, B. (2008), "Monitoring of electrically isolated post-tensioning tendons", *Tailor made concrete structures*, Taylor & Francis, London.

Fricker, S. and Vogel, T. (2007), "Site installation and testing of a continuous acoustic monitoring", *Constr. Build. Mater.*, **21**(3), 501-510.

Lanza di Scalea, F., Rizzo, P. and Seible, F. (2003), "Stress measurement and defect detection in steel strands by guided stress waves", *J. Mater. Civ. Eng.*, **15**(3), 219-227.

Lau, K., Lasa, I. and Paredes, M. (2013), "Corrosion failure of post-tensioned tendons in presence of deficient grout", *Proceedings of the NACE International CORROSION 2013*, Orlando, FL, March.

Liu, W., Hunsperger, R.G., Folliard, K., Chajes, M.J., Barot, J. and Jhaveri, D. (1999), "Detection and characterization of corrosion of bridge cables by time domain reflectometry", *Proceedings of the SPIE Nondestructive Evaluation of Bridges and Highways III*, Bellingham, WA.

Liu, W., Hunsperger, R.G., Chajes, M.J., Folliard, K.J. and Kunz, E. (2002), "Corrosion detection of steel cables using time domain reflectometry", *J. Mater. Civ. Eng.*, **14**(3), 217-223.

Marceau, D., Bastien, J. and Fafard, M. (2001), "Experimental and numerical studies of mono-strand anchorage", *Struct. Eng. Mech.*, **12**(2), 119-134.

Nguyen, K.D. and Kim, J.T. (2012), "Smart PZT-interface for wireless impedance-based prestess-loss monitoring in tendon-anchorage connection", *Smart Struct. Syst.*, **9**(6), 489-504.

Salamone, S., Bartoli, I., Phillips, R., Nucera, C. and Lanza di Scalea, F. (2011), "Health monitoring of prestressing tendons in posttensioned concrete bridges", *Transportation Research Record 2220*, Transportation Research Board, Washington, DC.

Salamone, S., Veletzos, M.J., Lanza di Scalea, F. and Restrepo, J.I. (2012), "Detection of initial yield and onset of failure in bonded posttensioned concrete beams", *J. Bridge Eng.*, **17**(6), 966-974.

Scheel, H. and Hillemeier, B. (2003), "Location of prestressing steel fractures in concrete", *J. Mater. Civ. Eng.*, **15**(3), 228-234.

Tabatabai, H., Mehrabi, A.B. and Yen, W.P. (1998), "Bridge stay cable condition assessment using vibration measurement techniques", *Proceedings of the SPIE Structural Materials Technology III: An NDT Conference*, Bellingham, WA.

Wang, M.L., Chen, Z.L., Koontz, S.S. and Lloyd, G.M. (2000), "Magnetoelastic permeability measurement for stress monitoring in steel tendons and cables", *Proceedings of the SPIE Nondestructive Evaluation of Highways, Utilities, and Pipelines IV*, Bellingham, WA.

Yuyama, S., Yokoyama, K., Niitani, K., Ohtsu, M. and Uomoto, T. (2007), "Detection and evaluation of failures in high-strength tendon of prestressed concrete bridges by acoustic emission", *Constr. Build. Mater.*, **21**(3), 491-500.

Zejli, H., Gaillet, L., Laksimi, A. and Benmedakhene, S. (2012), "Detection of the presence of broken wires in cables by acoustic emission inspection", *J. Bridge Eng.*, **17**(6), 921-927.

BS